



CPU parallel-based adaptive parameterized level set method for large-scale structural topology optimization

Hui Liu¹ · Peng Wei² · Michael Yu Wang³

Received: 28 June 2020 / Revised: 22 September 2021 / Accepted: 24 November 2021 / Published online: 6 January 2022
© The Author(s), under exclusive licence to Springer-Verlag GmbH Germany, part of Springer Nature 2022

Abstract

In this paper, an adaptive parameterized level set topology optimization method (APLSM) is proposed by using a bilinear basis function which is common in the finite element method (FEM) to parameterize the level set function. A CPU parallel computing strategy is applied for large-scale topology optimization problems. In the presented APLSM, the solving of an additional linear system, which is necessary for each iteration in the radial basis functions-based parametric level set method (PLSM), is completely avoided since the coefficient matrix of the system degenerates into an identity matrix when using the basis function to parameterize the level set function. In this way, the computational efficiency could be improved significantly. Furthermore, pattern repetition constraints are also imposed to design the graded hierarchical and cellular structures with high geometric complexity by using the proposed APLSM and parallel computing. Several numerical examples have been carried out for verifying the effectiveness of the proposed method. For two-dimensional examples, the computational efficiency is improved about 20% to 80% by comparison with the traditional compactly supported radial basis functions (CSRBFs)-based PLSM with different support radii. For the large-scale three-dimensional problems, the computational efficiency of the proposed method is also much higher. For a plate model meshed by more than 13 million 8-node hexahedral elements, only approximately 2 s in each iteration are consumed in all the calculation processes except for the solving of the structural static equilibrium equations, including the generating of mesh, the assembling of the element stiffness matrices, the imposing of the boundary conditions, and the updating of the level set function.

Keywords Structural topology optimization · Parallel computation · Parameterized level set method · Large-scale · Basis function

1 Introduction

A series of great progress has been made in structural topology optimization since the prominent research work of Bendsøe and Kikuchi (1988). By transforming the optimization problem of structural configuration into the evolution problem of a level set function, Wang et al. (2003) and Allaire et al. (2004) developed the level set-based topology optimization method, where the evolution of the level set function was determined by solving the Hamilton–Jacobi partial differential equation (HJ-PDE) and the boundary of the structure was represented by the zero isosurfaces of the level set function. In the past two decades, this method has been improved greatly and has been widely used in various optimization problems (Burger and Osher 2005; Gain and Paulino 2013; van Dijk et al. 2013; Sigmund and Maute 2013; Deaton and Grandhi 2014).

Responsible Editor: Ming Zhou

✉ Peng Wei
ctpwei@scut.edu.cn

¹ Department of Engineering Mechanics, School of Civil Engineering, Wuhan University, Wuhan, China

² School of Civil Engineering and Transportation, State Key Laboratory of Subtropical Building Science, Guangdong Provincial Key Laboratory of Technique and Equipment for Macromolecular Advanced Manufacturing, South China University of Technology, Guangzhou, China

³ Department of Mechanical and Aerospace Engineering, Hong Kong University of Science and Technology, Kowloon, Hong Kong

To avoid some issues caused by solving the HJ-PDE in the classical level set method, a parameterized level set method (Wang and Wang 2006; Wang et al. 2007) was developed. In this method, the level set function was parameterized by using radial basis functions (RBFs). Consequently, the boundary of the structure was updated by adjusting a set of coefficients of RBFs with fixed knots (Wei et al. 2018) or the locations of RBFs with dynamic knots (Ho et al. 2007). Due to the simplicity of numerical implementation, the RBFs with fixed nodes are often used in the parameterized level set method (Wei and Wang 2006; Luo et al. 2007, 2008).

The supported domain of RBFs can be global or local, i.e., global supported radial base functions (GSRBFs) or compact supported radial base functions (CSRBFs). By parameterizing the level set function with any spatial discretization method, such as the GSRBFs and CSRBFs, the HJ-PDE can be transformed into a set of ordinary differential equations (ODEs), which are much easier to solve.

However, in the calculation, another problem was raised, that is, an additional linear system needs to be solved during this parameterization process in each iteration step. The number of equations in the additional linear system is the same as the number of knots of the RBFs. When using the GSRBFs to parameterize the level set function, the coefficient matrix of the additional linear system is full, and it will become a sparse matrix when using the CSRBFs. Regardless of whether the GSRBFs or CSRBFs are used, the parameterization process will consume a lot of computing resources. To improve the computational efficiency of this parameterization process, Li et al. (2015) adopted a discrete wavelet transform (DWT) approximation to compress the coefficient matrix by reducing the number of its non-zero elements. Although this technique can improve the calculation efficiency to some extent, it still needs to solve the additional linear system in each iteration. For the same purpose, the partition of unity method was employed by Ho et al. (2011) in the parametric level set method to improve the efficiency. Recently, Liu et al. (2019a) provided a subdomain parametric level set method, where the parameterization process was conducted and the coefficient matrix can be obtained only on each subdomain independently. It should be mentioned that the level set function can also be parameterized by using the B-Spline functions (Wang et al. 2019), the non-uniform rational basis spline (NURBS) functions (Wang and Benson 2016; Jahangiry and Tavakkoli 2017), the cardinal basis functions (Jiang et al. 2018), etc.

In this work, an adaptive parameterized level set method is proposed by adopting the basis function used in the FEM to parameterize the level set function. Compared with the traditional GSRBFs- and CSRBFs-based parameterized level set methods, there is no longer a need to solve an additional linear system in each iteration step, which will save lots of computational resources. In our previous

proposed fully parallel CSRBFs-based parameterized level set method (Liu et al. 2019b), the establishment of the coefficient matrix of the additional linear system is very difficult. The number of non-zero elements in each row and column of the matrix is the same as the number of knots located in the support domain of the CSRBFs. Therefore, for different knot densities, the number of knots located in the support domain is different, which requires different memory spaces to be allocated for different rows and columns of the matrix. In this paper, the coefficient matrix of the additional linear system becomes an identity matrix for any non-uniform structured mesh or unstructured mesh, since the basis function is used to parameterize the level set function and it is non-zero only on their label knot. To verify the effectiveness of the proposed method further, the proposed method is extended to the topology optimization of large-scale/high-resolution structures by virtue of an open-source and high-performance parallel computing platform (PETSc, <https://www.mcs.anl.gov/petsc/>).

This paper is organized as follows. In the next section, the fundamentals of the adaptive parameterized level set method are presented. As a comparison, the traditional parameterization process using the GSRBFs or CSRBFs is also briefly introduced. Then, the optimization problem of minimum compliance is considered and the corresponding evolution velocity field of the parametric level set function is deduced in Sect. 3. Furthermore, in Sect. 4, some typical numerical examples are carried out for verifying the effectiveness of the proposed method. Finally, some conclusions are given in Sect. 5.

2 Adaptive parameterized level set method

In the level set method, the boundary of structure is represented by a level set function $\phi(\mathbf{x}, t)$, as illustrated in Fig. 1, i.e.,

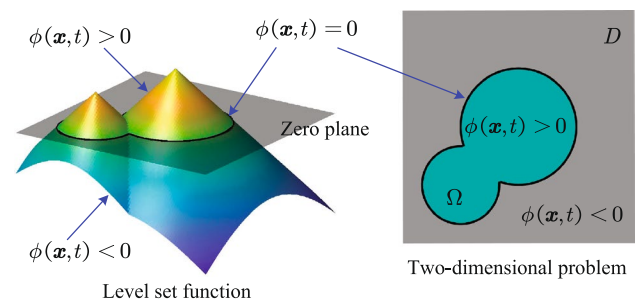


Fig. 1 Representing a two-dimensional problem with a level set function

$$\begin{aligned}
 \phi(\mathbf{x}, t) > 0 &\iff \forall \mathbf{x} \in \Omega \\
 \phi(\mathbf{x}, t) = 0 &\iff \forall \mathbf{x} \in \partial\Omega \\
 \phi(\mathbf{x}, t) < 0 &\iff \forall \mathbf{x} \in D \setminus (\Omega \cup \partial\Omega)
 \end{aligned}
 \tag{1}$$

where t , D , Ω , and $\partial\Omega$ represent the artificial time, the design domain, the structure domain, and the boundaries of structure, respectively.

By using the level set function, the evolution of structural boundaries is transformed into the updating of the zero iso-surfaces of the level set function implicitly. In the classical level set method (Wang et al. 2003; Allaire et al. 2004), the evolution of level set function is achieved by solving the HJ-PDE, i.e.,

$$\frac{\partial \phi(\mathbf{x}, t)}{\partial t} - \vartheta^n |\nabla \phi(\mathbf{x}, t)| = 0
 \tag{2}$$

with ϑ^n being given by

$$\vartheta^n = -\frac{d\mathbf{x}}{dt} \cdot \frac{\nabla \phi(\mathbf{x}, t)}{|\nabla \phi(\mathbf{x}, t)|}
 \tag{3}$$

where $\vartheta^n = \vartheta^n(\mathbf{x}, t)$ denotes the normal velocity field of the zero iso-surfaces of the level set function and it depends on the shape derivative of the objective function of the optimization problem.

In the classical level set method, the level set function is updated by solving the above-mentioned HJ-PDE in every iteration step. This will cause some main issues which have been pointed out in our previous work (Wei et al. 2018):

- The level set function must be re-initialized frequently to maintain a signed distance function, which is important to keep the normal gradient of the level set function constant.
- The time step size must be sufficiently small to satisfy the Courant–Friedrichs–Lewy (CFL) condition for numerical stability since the explicit time integration scheme is usually used for solving the HJ-PDE.
- The classical level set method cannot create new holes (Xia et al. 2019), which makes it easy to fall into the local optimal solution space.

To overcome these shortcomings, the parameterized level set method (Wang and Wang 2006; Wang et al. 2007) is developed by treating the level set function as a linear combination of a series of radial basis functions. Generally, the radial basis functions are fixed and do not change during optimization. Only their coefficients are related to artificial time and can be changed. In this way, the level set function can be evolved by adjusting the coefficients of the radial basis functions. In addition, the capability of hole nucleation is also improved greatly in the framework of PLSM, as studied in our previous work (Wei et al. 2018).

In fact, in addition to the radial basis functions, we can also choose other functions to parameterize the level set function. In this paper, the basis function used in the FEM is employed since it can make the parameterization process much easier.

Without loss of generality, suppose here that a set of functions $\psi_i(\mathbf{x})$ and their coefficients $\alpha_i(t)$ are employed to parameterize the level set function, i.e.,

$$\phi(\mathbf{x}, t) = \sum_{i=0}^m \psi_i(\mathbf{x}) \alpha_i(t)
 \tag{4}$$

in which m is the number of knots.

Substituting Eq. (4) into Eq. (2) leads to

$$\boldsymbol{\psi}(\mathbf{x})^T \frac{d\boldsymbol{\alpha}(t)}{dt} - \vartheta^n |\nabla \boldsymbol{\psi}(\mathbf{x}) \boldsymbol{\alpha}(t)| = 0,
 \tag{5}$$

where $\boldsymbol{\psi}(\mathbf{x}) = \{\psi_1(\mathbf{x}), \psi_2(\mathbf{x}), \dots, \psi_m(\mathbf{x})\}^T$ and $\boldsymbol{\alpha}(t) = \{\alpha_1(t), \alpha_2(t), \dots, \alpha_m(t)\}^T$.

Furthermore, Eq. (5) can also be discrete on the knots, i.e.,

$$\mathbf{H} \frac{d\boldsymbol{\alpha}(t)}{dt} - \mathbf{v}(\boldsymbol{\alpha}(t), t) = 0,
 \tag{6}$$

where \mathbf{H} and \mathbf{v} can be called the parameterization matrix and the evolution velocity vector, respectively. They can be written as

$$\mathbf{H} = \begin{bmatrix} \psi_1(\mathbf{x}_1) & \psi_2(\mathbf{x}_1) & \dots & \psi_m(\mathbf{x}_1) \\ \psi_1(\mathbf{x}_2) & \psi_2(\mathbf{x}_2) & \dots & \psi_m(\mathbf{x}_2) \\ \vdots & \vdots & \ddots & \vdots \\ \psi_1(\mathbf{x}_m) & \psi_2(\mathbf{x}_m) & \dots & \psi_m(\mathbf{x}_m) \end{bmatrix}
 \tag{7}$$

$$\mathbf{v} = \left\{ \begin{array}{l} \vartheta^n(\mathbf{x}_1, t) |\nabla \boldsymbol{\psi}(\mathbf{x}_1) \boldsymbol{\alpha}(t)| \\ \vartheta^n(\mathbf{x}_2, t) |\nabla \boldsymbol{\psi}(\mathbf{x}_2) \boldsymbol{\alpha}(t)| \\ \vdots \\ \vartheta^n(\mathbf{x}_m, t) |\nabla \boldsymbol{\psi}(\mathbf{x}_m) \boldsymbol{\alpha}(t)| \end{array} \right\}
 \tag{8}$$

When the gradient of level set function at the structural boundary is normalized by using $|\nabla \phi(\mathbf{x}, t)| = |\nabla \boldsymbol{\psi}(\mathbf{x}) \boldsymbol{\alpha}(t)| = 1$, the velocity field in Eq. (8) becomes

$$\mathbf{v} = \{ \vartheta^n(\mathbf{x}_1, t) \ \vartheta^n(\mathbf{x}_2, t) \ \dots \ \vartheta^n(\mathbf{x}_m, t) \}^T
 \tag{9}$$

The condition of $|\nabla \phi| = 1$ requires that the level set function is a sign distance function at least around the boundary. A strategy (Wei et al. 2018) is adopted to make this requirement approximately satisfied. In addition, an approximate function (Wei et al. 2018) is employed to limit the normal velocity ϑ^n around the zero iso-surfaces of the level set function for improving the stability of the algorithm. Then, the velocity field in Eq. (9) finally can be re-written as

$$v = \begin{Bmatrix} \vartheta^n(x_1, t)\delta(\phi(x, t)) \\ \vartheta^n(x_2, t)\delta(\phi(x, t)) \\ \vdots \\ \vartheta^n(x_m, t)\delta(\phi(x, t)) \end{Bmatrix}. \tag{10}$$

By using the first-order difference scheme for solving Eq. (6), we have

$$H\gamma_k = v(\alpha(t_k), t_k) \tag{11}$$

$$\alpha(t_{k+1}) = \alpha(t_k) + \Delta t \gamma_k, \tag{12}$$

where γ_k is a temporary variable to be solved, t_k is the k th time step, and Δt is the time step size. For the initial moment ($t_0 = 0$), we have

$$\alpha(t_0) = H^{-1}\phi(t_0) \tag{13}$$

with $\phi(t_0) = \{\phi(x_1, t_0), \phi(x_2, t_0), \dots, \phi(x_m, t_0)\}^T$.

In the computation, the additional linear system, i.e., Eq. (11), needs to be solved in every iteration step (Liu et al. 2019b; Wei et al. 2020). Furthermore, the parameterization matrix H will become a full matrix which takes up lots of computer memory, when using the GSRBFs to parameterize the level set function, such as the MultiQuadric spline functions. To reduce the computational cost, the CSRBFs, such as the C^2 Wendland functions (Wendland 1995), are usually employed and the matrix H will become a sparse matrix whose number of non-zero elements closely depends on the support radius and knot density distribution of the CSRBFs.

As illustrated in Fig. 2a, 21×21 knots are uniformly distributed in the global domain $[-1, 1] \times [-1, 1]$. Each knot is represented by a small black dot. The number of the non-zero points of different radial basis functions (the GSRBFs and CSRBFs) at the i -th knot marked with a solid red circle is investigated. It should be mentioned that the number of the non-zero points of the radial basis function at the i -th knot is the same as the number of non-zero elements in the

corresponding i -th row and column of the parameterization matrix H . For the GSRBFs, all the non-zero points are marked by red hollow circles shown in Fig. 2b. For the CSRBFs, only the points in the support domain with r_s being the radius are marked as shown in Fig. 2c.

When using the basis function $N_i(x)$ to parameterize the level set function, i.e., let $\psi_i(x) = N_i(x)$, the matrix H will degenerate into an identity matrix, since the basis function has the property $N_i(x_j) = \delta_{ij}$, where δ is the Kronecker symbol, i.e.,

$$N_i(x_j) = \begin{cases} 1, & \text{if } i = j \\ 0, & \text{if } i \neq j \end{cases} \tag{14}$$

The single non-zero point of the basis function is marked on their label knot as shown in Fig. 2d.

By using the basis function to parameterize the level set function, Eq. (11) and Eq. (12) become

$$\phi(t_{k+1}) = \phi(t_k) + \Delta t v(\phi(t_k), t_k) \tag{15}$$

with $\phi(t_k) = \{\phi(x_1, t_k), \phi(x_2, t_k), \dots, \phi(x_m, t_k)\}^T$.

3 Optimization problem

The minimum compliance problem is considered in the present study and its optimization formulation can be given by

$$\begin{aligned} \min_{\phi, u} : & J(\phi, u) = \int_{\Omega(\phi)} f \cdot u d\Omega + \int_{\partial\Omega_\sigma(\phi)} \tau \cdot u dS \\ \text{s.t.} : & a(u, w) = \ell(w), \forall w \in U \\ & u = \bar{u}, \text{ on } \partial\Omega_u \\ & \sigma = \tau, \text{ on } \partial\Omega_\sigma \\ & V - \bar{V} \leq 0 \end{aligned}, \tag{16}$$

where $J(u)$ is the compliance of structure; $a(u, w) = \ell(w)$ is the weak form for the linear elasticity problem; $V = \int_{\Omega} d\Omega$ denotes the material volume of the current structure; \bar{V} is a user-specified maximum material volume usage; f, u , and

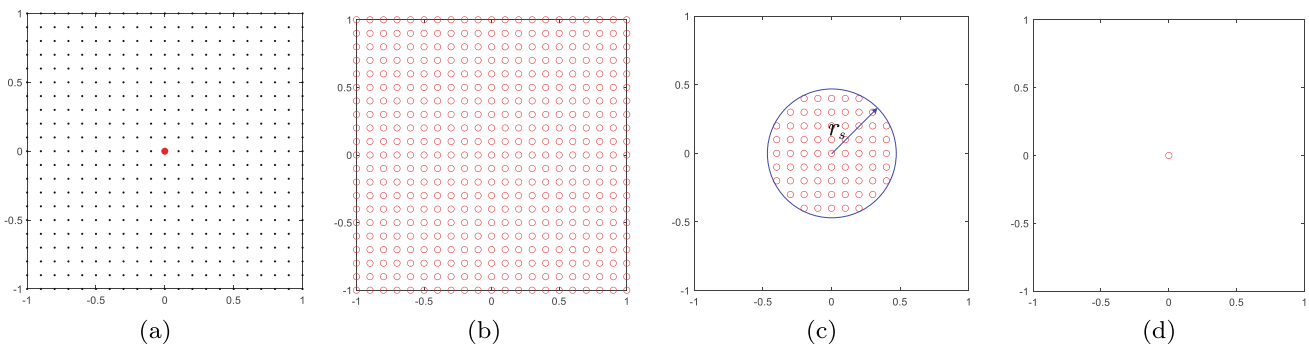


Fig. 2 Illustration of non-zero points of different functions: **a** knot distribution and the i -th knot marked with a solid red circle; **b** non-zero points of the GSRBF at the i -th knot; **c** non-zero points of the

CSRBF at the i -th knot with r_s being the radius of its support domain; **d** single non-zero point of the basis function at the i -th knot

σ represent the body force, displacement, and stress, respectively; \bar{u} is the specified displacement on the displacement boundary and τ is the specified stress on the stress boundary. The definition of the two-dimensional problem is illustrated in Fig. 3.

For the minimum compliance problem, if the body force and boundary traction are neglected, the normal velocity field ϑ^n of the zero isosurfaces of the level set function is related to the strain energy density and a Lagrange multiplier in the gradient-based optimization formulation (Wang et al. 2003; Allaire et al. 2004; Wei et al. 2018), i.e.,

$$\vartheta^n(\mathbf{x}) = E_{ijkl}\epsilon_{ij}(\mathbf{x})\epsilon_{kl}(\mathbf{x}) - \lambda \tag{17}$$

in which E_{ijkl} is the fourth-order elastic tensor; ϵ_{ij} is the second-order strain tensor; λ is the Lagrange multiplier to deal with the constraint on the material volume.

In the parameterized level set method, the level set function can be updated by using Eq. (12) or Eq. (15) with ϑ^n being obtained from Eq. (17). Figure 4 shows the calculation flowcharts of the two schemes of the parameterized level set methods based on the radius basis function and the basis function, respectively. From Fig. 4, we can see that the generation of the matrix \mathbf{H} and the solving of the linear equations for parameterization, i.e., the calculation processes with red color and dashed boxes shown in Fig. 4a, are completely avoided in the proposed method by comparison with the traditional GSRBFs- and CSRBFs-based parameterized level set methods.

It should be mentioned that the same mesh is employed for the spatial discretization of the level set function and the finite element analysis of the design domain during the optimization process. Therefore, the numbers of coefficients used in the CSRBF-based PLSM and the proposed APLSM are the same. In addition, the reference mesh remains fixed during the whole optimization. According to Eq. (1), the whole design domain is divided into three parts by the level set function, i.e., the structure (solid) domain Ω , the boundary of structure $\partial\Omega$, and the weak material domain $D \setminus (\Omega \cup \partial\Omega)$. Correspondingly, three kinds of elements with different elastic constants are employed in the finite element

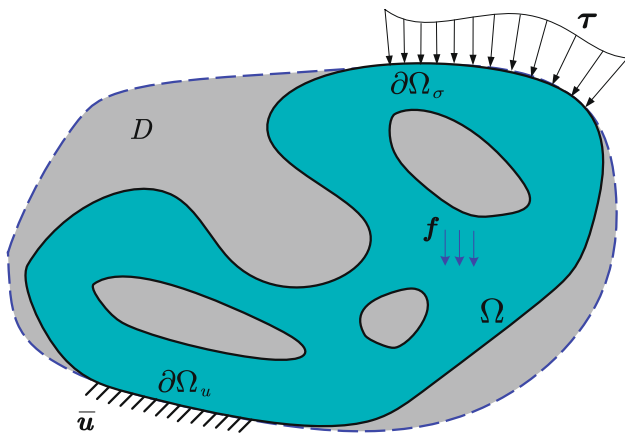
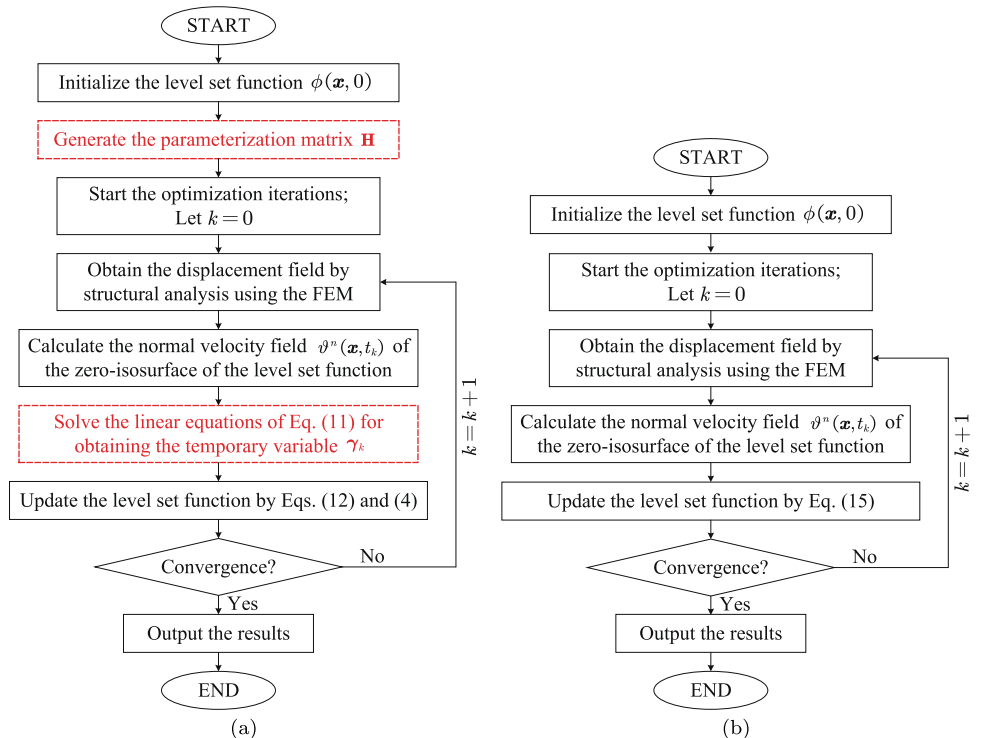


Fig. 3 Definition of a two-dimensional structure in the optimization problem

Fig. 4 Calculation flowcharts: a the traditional GSRBFs- and CSRBFs-based parameterized level set methods; b the proposed basis function-based parameterized level set method



analysis, i.e., the solid element with $\rho_e = 1$, the blending element with $0 < \rho_e < 1$, and the weak element with $\rho_e = 0$, where ρ_e represents virtual element density. As illustrated in Fig. 5a, the solid element is completely covered by the structure domain and the weak element is completely located in the weak material domain, while the blending element is crossed by the zero-isosurface of the level set function. For the blending elements, ρ_e can be calculated by

$$\rho_e = \frac{\int_{D_e} H(\phi) d\Omega}{\int_{D_e} d\Omega} = \frac{\sum_{p=1}^{6^{\text{dim}}} H(\phi(\xi_p)) |\mathbf{J}_e(\xi_p)| w_p}{\sum_{p=1}^{2^{\text{dim}}} |\mathbf{J}_e(\xi_p)| w_p}, \quad (18)$$

where $H(x)$ indicates the Heaviside function; \mathbf{J}_e represents the Jacobian matrix of element; ξ_p denotes the coordinate vector of Gaussian integration point; w_p means the integration weight factor; D_e means the domain of element; the superscript 'dim' denotes dimension of the optimization problem. 'dim' is equal to 2 for plane problem, 3 for spatial problem.

By using the definition of Eq. (18), the virtual densities of all elements can be calculated as shown in Fig. 5b. Then, the stiffness matrix of each element \mathbf{k}_e can be given by

$$\mathbf{k}_e = [E_w + \rho_e(E_s - E_w)] \mathbf{k}_0, \quad (19)$$

where \mathbf{k}_0 represents the stiffness matrix of the solid element with unit Young's modulus; E_s denotes Young's modulus of solid material; and E_w is a positive small quantity used to represent the elastic modulus of weak material. $E_w = 10^{-9} E_s$ is adopted in this paper.

To assess the computational accuracy of this projection approach, the strain energy distribution, as shown in Fig. 5c, is obtained by using the finite element analysis (FEA) based on the fixed coarse regular mesh with 60×30 quadrilateral four-node (Q4) elements. For the results of the optimized structure with fixed coarse mesh, vertical displacement of the node at the midpoint on the right end is $V_{\text{fixed}} = -59.46$, the maximum strain energy of the node is $S_{\text{fixed}} = 0.50$, and the compliance is $J_{\text{fixed}} = 59.92$. As a comparison, the FEA is also conducted for the optimized structure with refined unstructured body-fitted mesh as shown in Fig. 6a, where 11583 triangular three-node (T3) elements and 6465 nodes are used. Other calculation parameters are the same for the fixed coarse regular mesh and the refined body-fitted mesh. The strain energy distribution of the optimized structure with body-fitted mesh is presented in Fig. 6b, where the maximum strain energy of the node is $S_{\text{fitted}} = 0.57$. In addition, the vertical displacement of the node at the midpoint on the right end is $V_{\text{fitted}} = -59.56$ and the corresponding compliance is $J_{\text{fitted}} = 59.46$. Their relative errors are $V_{\text{err}} = \frac{|V_{\text{fixed}} - V_{\text{fitted}}|}{|V_{\text{fitted}}|} \times 100\% = 0.17\%$ and $J_{\text{err}} = \frac{|J_{\text{fixed}} - J_{\text{fitted}}|}{|J_{\text{fitted}}|} \times 100\% = 0.77\%$, respectively. The relative error of the maximum strain energy is a bit large due to the high stress concentration in the upper and lower local areas of the left end of the structure, i.e., $S_{\text{err}} = \frac{|S_{\text{fixed}} - S_{\text{fitted}}|}{|S_{\text{fitted}}|} \times 100\% = 12.28\%$. From this comparison, we can see that the calculation accuracy of the simple projection method used in this paper is reliable and efficient. Actually, this approach is usually

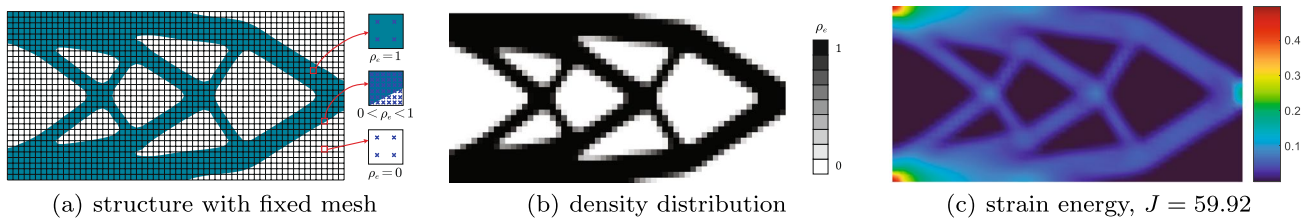


Fig. 5 Geometry configuration, density distribution, and strain energy of the optimized structure based on the fixed mesh

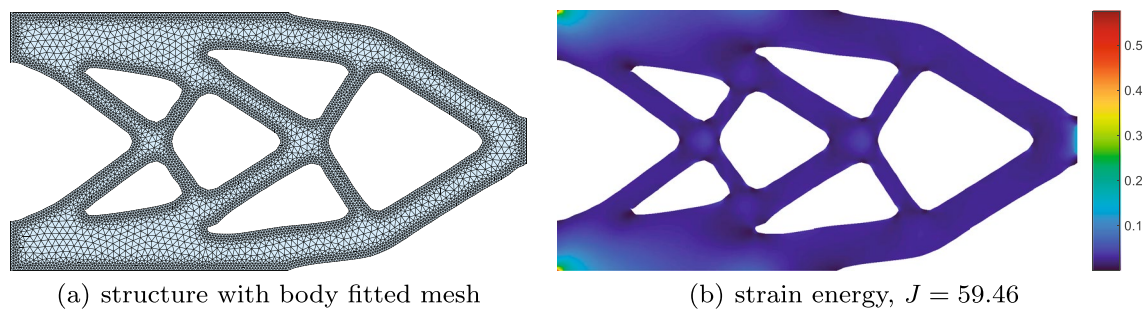


Fig. 6 Refined unstructured body-fitted mesh and strain energy of the optimized structure

adopted in the level set-based structural topology optimization (Luo et al. 2008; Xia and Shi 2015; Liu et al. 2020).

4 Numerical examples

Several typical numerical examples are carried out in this section for verifying the effectiveness of the proposed adaptive parameterized level set method (APLSM). Hierarchical structures usually have the same microstructure in one or two of the dimensions. In this work, a repetition constraint is also introduced herein for designing the hierarchical structures and it is illustrated in Fig. 7. In addition, these structures usually have extremely high geometric complexity. Thus, the parallel computing technology is used for optimizing the hierarchical structures. When applying the repetition constraint (Liu et al. 2018), the design domain D is divided into a set of subdomains D_q^p with $q = 1, 2, \dots, Q$ and $p = 1, 2, \dots, P$, where Q and P are the numbers of subdomains in the x direction and the y direction, respectively. When applying the repetition constraint in the x direction, we only need to make

$$(\vartheta^n)_1^p = (\vartheta^n)_2^p = \dots = (\vartheta^n)_Q^p = \frac{1}{Q} \sum_{q=1}^Q (\vartheta^n)_q^p, \tag{20}$$

where $(\vartheta^n)_q^p$ means the normal velocity ϑ^n at the local position of the subdomain D_q^p . Similarly, the repetition constraint can be also applied in the y direction as

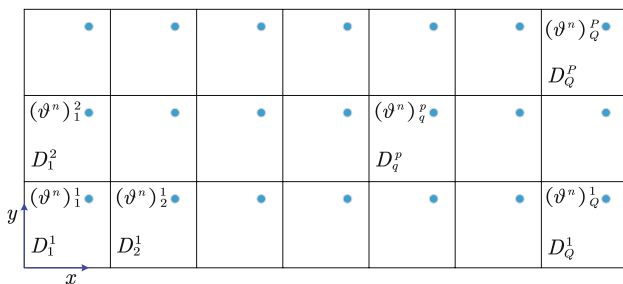


Fig. 7 Schematic diagram of applying repetition constraint

$$(\vartheta^n)_q^1 = (\vartheta^n)_q^2 = \dots = (\vartheta^n)_q^P = \frac{1}{P} \sum_{p=1}^P (\vartheta^n)_q^p. \tag{21}$$

Furthermore, generalized symmetry constraints can also be imposed in this manner. Interested readers can refer to our previous work (Liu et al. 2018) for more details.

In the following numerical examples, Young’s modulus of solid material is set as $E_s = 1Pa$ and it is $E_w = 10^{-9}Pa$ for the weak material. In addition, the Poisson’s ratios for all examples are the same, i.e., $\mu = 0.3$.

4.1 Comparison of optimized structures by the traditional method and the proposed method

As shown in Fig. 8, an MBB beam model, a cantilever beam model, and a Michell-type model are designed by using both the traditional parameterized level set method (PLSM) based on the CSRBFs with different support radii and the proposed APLSM. All the quantities are dimensionless. $L = 210$ and $W = 70$ for the MBB model and they are $L = 180$ and $W = 90$ for the cantilever beam model and the Michell-type model. In these three models, their external forces and the upper bounds of the maximum material volume usage ratios are set to $F = 1$ and $v_f = 0.5$, respectively. Due to the symmetry of the MBB model, only half of the model is considered. The meshes used for these three models are 210×70 , 180×90 , and 180×90 , respectively. For comparison purposes, two different support radii $r_s = 2$ and $r_s = 8$ are considered in the traditional CSRBFs-based PLSM for studying the effect of support radius on computing time of the parameterization process. In this example, all the models are calculated on the same computer equipped with Inter(R) Core(TM) i7-8550U CPU and 16G RAM.

The initial designs are shown in Fig.9a and f. The optimized structures of the MBB beam problem are shown in Fig.9b ~ Fig.9d and those of the cantilever beam problem are given in Fig.9g ~ Fig.9h. The optimized structure in Fig. 9b is obtained by using the CSRBFs-based PLSM with support radius being $r_s = 2$. The number of iteration steps is $N_{steps} = 504$ and the average computing time for

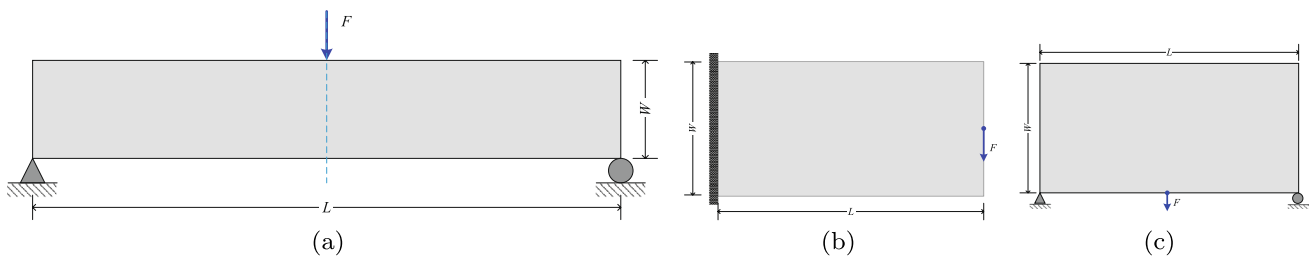


Fig. 8 Computational models and their boundary conditions: a MBB beam model; b Cantilever beam model; c Michell-type structure

each iteration is $t_{average} = 0.55s$. The structure in Fig. 9c is designed by using the PLSM based on the CSRBFs with $r_s = 8$. $N_{steps} = 508$ and $t_{average} = 1.72s$ for Fig. 9c. While for the optimized structure in Fig. 9d obtained by using the proposed APLSM, $N_{steps} = 501$ and $t_{average} = 0.44s$, which indicates that the computation efficiency per iteration is improved by about 20% and 74% by comparison with the results in Fig. 9b and Fig. 9c, respectively. Similar conclusions can also be drawn from the comparison of the optimization results of the cantilever beam model. The optimized structures shown in Fig. 9g are obtained by using the PLSM based on the CSRBFs with support radii $r_s = 2$ and $r_s = 8$. The average computing time per iteration is $t_{average} = 0.62s$ and $t_{average} = 2.46s$, respectively. While for the optimized structure calculated by using the proposed APLSM, as shown in Fig. 9h, its average time is only about $t_{average} = 0.44s$, which means that the computational efficiency for the cantilever beam model is improved by 29% and 82% appropriately. For the Michell-type structure, the average computing time per iteration of the results obtained by the proposed method and the CSRBFs-based PLSM with $r_s = 2$ and $r_s = 8$ are 0.32s, 0.42s, and 1.52s, respectively. Thus, the computational efficiency is improved by about 24% and 79% by comparison with the CSRBFs-based PLSM with $r_s = 2$ and $r_s = 8$, respectively. From the comparison in this example, we can see that our new proposed APLSM has higher computational efficiency since the parameterization process is completely removed.

It should be noted that some small features may appear in the optimized structures as shown in Fig. 9a ~ Fig. 9d. In these regions, there are only blending elements that are crossed by the zero isosurfaces of the level set function. For these elements, the level set function values at some nodes are positive, and they are negative at the other nodes. In this case, the virtual densities of those blending elements are distributed between 0 and 1, which can be seen in Fig. 9e. These small features can be removed by using some implicit (Yaghmaei et al. 2020; Chen et al. 2021) or explicit (Guo et al. 2014; Xia and Shi 2015) size control algorithms.

4.2 Design of large-scale/high-resolution structures

To solve large-scale/high-resolution structural topology optimization problems in the parameterized level set design framework, the proposed method is implemented on the PETSc, a high-performance scientific computing platform.

For the GSRBF-based PLSM, the parameterization matrix \mathbf{H} is a full matrix that will consume a lot of computer memory and computing time, especially for the three-dimensional problems. Therefore, the CSRBFs-based parameterized level set method is usually used for large-scale structural topology optimization (Liu et al. 2019b) due to the less computational resources consumed in its parameterization process. Since the proposed APLSM in this paper avoids this process, its calculation is expected to be more efficient.

Compared with our previous work (Liu et al. 2019b), the pre-allocated memory space and generation of the

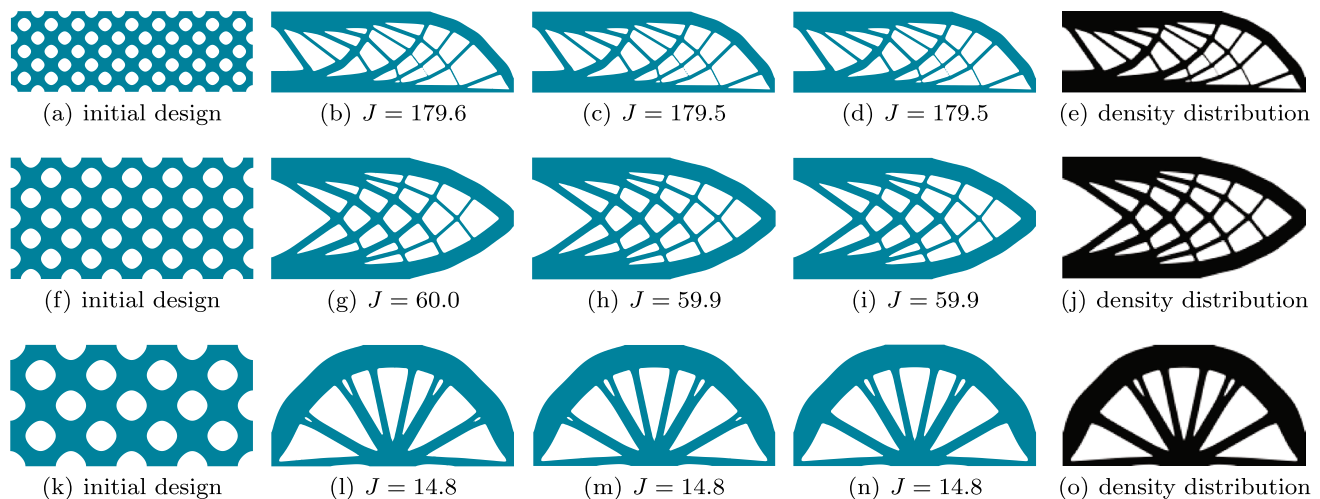


Fig. 9 Comparison of the optimized results: **a** initial design of the MBB beam; **b** optimized MBB beam by using the CSRBF-based PLSM with $r_s = 2$; **c** optimized MBB beam by using the CSRBF-based PLSM with $r_s = 8$; **d** optimized MBB beam by using the proposed APLSM; **e** element density distribution of the optimized structure shown in **(d)**; **f** initial design of the cantilever beam model; **g** optimized cantilever beam by using the CSRBF-based PLSM with $r_s = 2$; **h** optimized cantilever beam by using the CSRBF-based

PLSM with $r_s = 8$; **i** optimized cantilever beam by using the proposed APLSM; **j** element distribution of the optimized structure shown in **i**; **k** initial design of the Michell-type structure; **l** optimized Michell-type structure by using the CSRBF-based PLSM with $r_s = 2$; **m** optimized Michell-type structure by using the CSRBF-based PLSM with $r_s = 8$; **n** optimized Michell-type structure by using the proposed APLSM; **o** element density distribution of the optimized structure shown in **(n)**

parameterization matrix \mathbf{H} , the solving of Eq. (11) in each iteration and the coefficient vector α of CSRBFs are no longer needed in the proposed method. In this way, the parallel calculation program of the proposed method is very convenient to implement. In this work, the whole calculation processes are parallelized, including the generation of mesh, the calculation and integration of element stiffness matrix, the structural analysis by using the FEM, the computation of the normal velocity field ϑ^n , the updating of level set function, and the outputting of optimization results. The implementation details are the same as our previous work (Liu et al. 2019b), such as the mesh generation, the selection of integral points, and the post-processing.

In the PETSc computing platform, many kinds of sparse linear system solvers are available, including parallel and sequential, direct, and iterative. The combination of a Krylov subspace method and a preconditioner is popular for the iterative solution of linear systems. In this paper, the Flexible Generalized Minimal Residual method (Saad 1993) in conjunction with a multigrid preconditioner is employed in the structural analysis.

In this subsection, two design problems are solved by using the proposed APLSM and the traditional CSRBFs-based PLSM. Their computational models and boundary conditions are shown in Fig. 10, where all parameters are assumed to be dimensionless, i.e., $H = 96$ and $F = 1$ for Fig. 10a, $L = 1280$, $H = 32$ and $F = 4$ for Fig. 10b. Since the design domain and its boundary conditions are all symmetrical about the x and y axes, only one-quarter of the design domain is used for calculation. The meshes of $384 \times 192 \times 96$ and $640 \times 640 \times 32$ are employed for the optimizations of the cantilever beam model and the one-quarter of the plate model, respectively. In addition, the upper bounds of the volume fractions of the allowable material usages for these two models are set as 12% and 20%. For the plate model, the regions with a distance of $\frac{1}{32}H$ from the upper and lower surfaces are undesignable domains. These two optimization problems are conducted on a computer cluster, where each computer node is equipped with two Intel(R) Xeon(R) CPU E5-2678 v3 @ 2.50GHz and 64GB of RAM. For the cantilever beam model, 6 computer nodes with a totally of 144 processors

are occupied. While for the plate model, 15 computer nodes and 360 processors are used.

For the optimization problem in Fig. 10a, it converged after 172 iterations by using the proposed APLSM and the total computing time is about 2.7 h. The average calculation time per iteration step is about 56.5 s where 54 s are used to solve the linear system of the structure based on the Flexible Generalized Minimal Residual method and the multigrid preconditioner. The remaining 2.5 s are consumed during the other processes including the mesh generation, the assembly of element stiffness matrices, the imposition of boundary conditions, and the evolution of the level set function. The corresponding optimized configuration is shown in Fig. 11b. For comparison, the optimized result obtained by using the traditional PLSM is also presented in Fig. 11a. We can see that the two optimized configurations are almost the same, which indicates the correctness and effectiveness of the proposed APLSM once again.

For the optimization problem of the plate model shown in Fig. 10b, it converged after 182 iterations and the total consumed time is approximately 6 h. The average calculation time per iteration is about 119 s where more than 117 s are consumed by the finite element structural analysis and the remaining calculation time of fewer than 2 s is used for generating the meshes, assembling the element stiffness matrices, imposing the boundary conditions, and updating the level set function. As shown in Fig. 12, the whole configuration of the plate is obtained by reflecting the quarter of the plate optimized by using the proposed APLSM. From the internal views, we can see that a lot of very small truss-like structures with certain distribution rules appear in the sandwich domain of the plate.

4.3 Optimization of a bridge model with two different displacement constraints

A bridge model, whose design domain and boundary conditions are shown in Fig. 13, is optimized by using the proposed method under two different displacement constraints. For the first case (Case I), two edges at $x = 0$ and $x = 4W$ on the bottom surface of the design domain are clamped. For the second case (Case II), all the degrees of freedom of the nodes around the four corners of the lower surface of the

Fig. 10 Two computational models and their boundary conditions

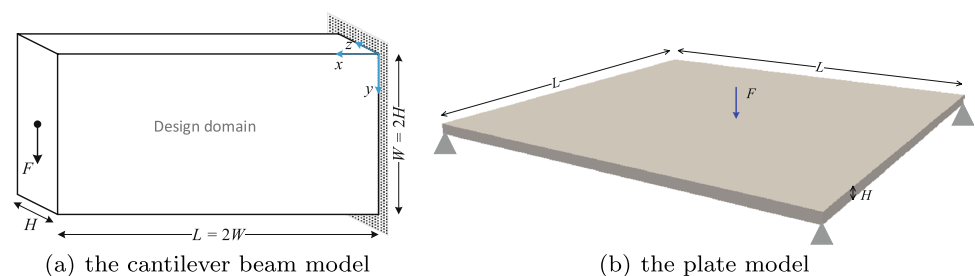


Fig. 11 Comparison of the optimized cantilever beams

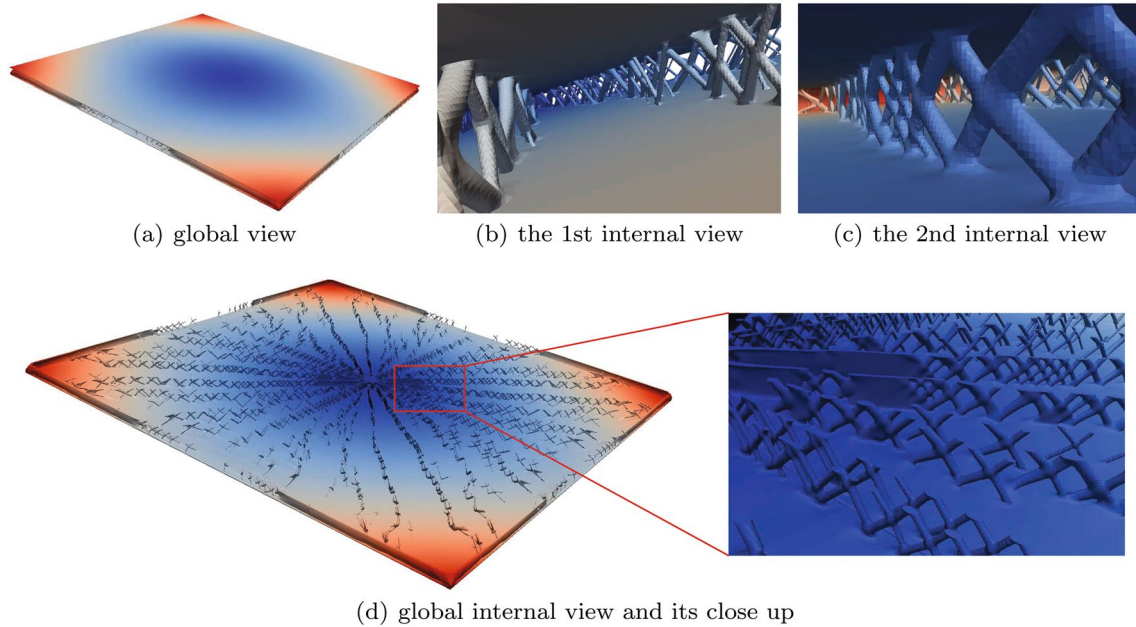
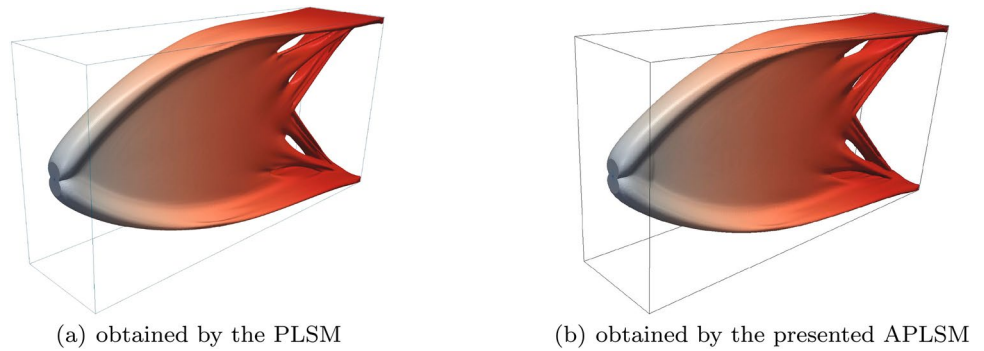


Fig. 12 Optimized plate and its local features (colored by the displacement field in the direction of plate thickness)

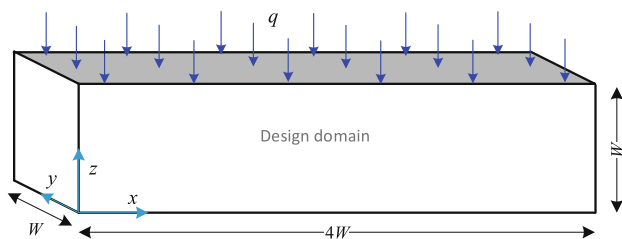


Fig. 13 Design domain and boundary conditions of the bridge model

design domain are constrained. A uniform distributed force q is imposed on the upper surface of the design domain. The domain less than $W/64$ from the top surface is undesignable. Only half of the model is calculated in this example because of symmetry. For the two cases, half of the design domain is divided into a uniform grid of $256 \times 128 \times 128$. Material properties of Young's modulus $E = 1$ and Poisson's

ratio $\mu = 0.3$ are used in this example. For Case I and Case II, the upper limits of volume fraction are set to 12% and 10%, respectively. The optimized results are presented in Fig. 14. Figure 14a, b, and c shows the optimized bridge and its features obtained under the fixed displacement constraints of the edges at $x = 0$ and $x = 4W$ on the lower surface of the design domain. Figure 14d, e, and f presents the results obtained under the fixed displacement constraints around the four corner points on the lower surface of the design domain.

4.4 Design of the structures with repetition constraints

In this subsection, two rotary-like structures are firstly designed by using the proposed APLSM with considering the repetition constraints. The two design models and their boundary conditions are shown in Fig. 15. As shown in Fig. 15a and c, pure torsional loads and corresponding

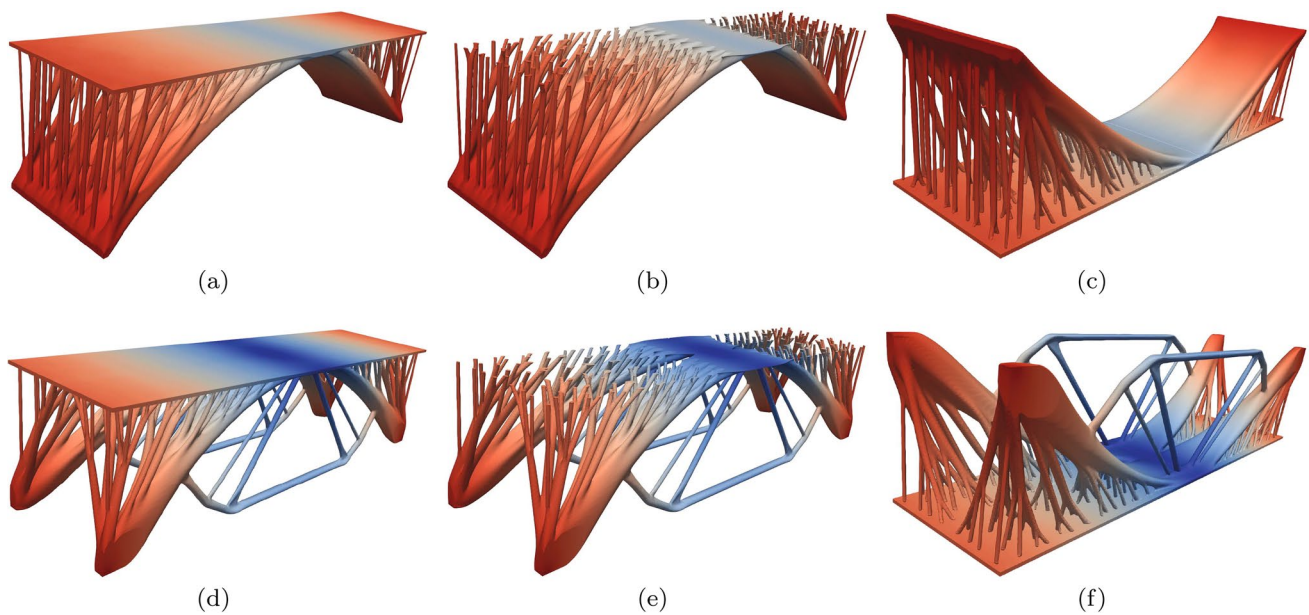


Fig. 14 Optimized bridges and images of these results from different perspectives (colored by the displacement field in the z direction): **a–c** are the optimized bridge and its features obtained under the dis-

placement constraints of Case I; **d–f** are the results obtained under the fixed displacement constraints of Case II

fixed displacement constraints are applied to both ends of the design domains of the cylinder-like and vase-like structures. In addition, their initial designs are presented in Fig. 15b and d, respectively. In this subsection, the numbers of three-dimensional 8-node hexahedral elements in all of the computation models are the same, which is $576 \times 8 \times 576$ in the height, thickness, and circumferential directions. The calculations for the models in this subsection are all carried out on the same workstation equipped with 48 CPU cores and 256 GB RAM.

The optimization results are shown in Figs. 16 and 18, where the repetition constraints are imposed in the circumferential direction with the different numbers of repeating patterns. In Fig. 16, except that the upper limit of the volume ratio in Fig. 16a is 0.15, those of other models are all 0.3. The numbers of repeating patterns $N_{patterns}$ of the optimized cylinder-like structures in Fig. 16a, b, c, and d are 6, 12, 24, and 24, respectively. From Fig. 16, we can see that the optimization results will become a thin-walled cylinder structure with the increase in the number of repeating patterns. However, when the upper limit of the amount of usable material is reduced, the optimal structure becomes a truss-like cylindrical structure as shown in Fig. 16d, whose internal view is given in Fig. 17. From the optimization results, we can deduce that for the design of the gyroscopic design models with pure torsional load, the thin wall structure has better force transmission performance when the allowable material amount is sufficient. However, when the maximum allowable material amount becomes small, the truss-like structure will

appear in the optimization result if the element size is not fine enough.

For the vase-like structure design problem, the numbers of repeating patterns $N_{patterns}$ of the optimized vase-like structures shown in Fig. 18 are set as 6, 12, and 24, respectively. From Fig. 18, we can find that the hole size of the designed truss-like structure becomes smaller and the lattice of the truss becomes denser when the number increases. This shows that if we continue to increase the number of repetitions, the optimized vase-like structure will also become a thin-walled structure, as long as the element size is fine enough. It should be mentioned that these conclusions are consistent with the conclusions in the work conducted by Sigmund et al. (2016).

A simply supported plate as shown in Fig. 19 considering the repeat pattern constraints in the x and y directions is carried out herein for further verifying the effectiveness of the proposed method. A uniform distributed force q is imposed on the top surface of the design domain. The upper limit of volume fraction is set as 30%. The whole design domain is meshed by $320 \times 320 \times 32$ with the number of repeating patterns being $N_{patterns} = 20$ in the x and y directions, while there is no repeat pattern constraint in the z direction. The optimized plate as shown in Fig. 20 is obtained by using the proposed APLSM with the repeat pattern constraints. The result indicates that the sandwich structure with periodic microstructure can be easily designed by using the presented topology optimization method with considering the repetition constraints.

Fig. 15 Computational models and their boundary conditions: **a** Cylindrical model with multiple torsional loads; **b** Initial design for the cylindrical model; **c** Vase-like model with multiple torsional loads; **d** Initial design for the vase-like model

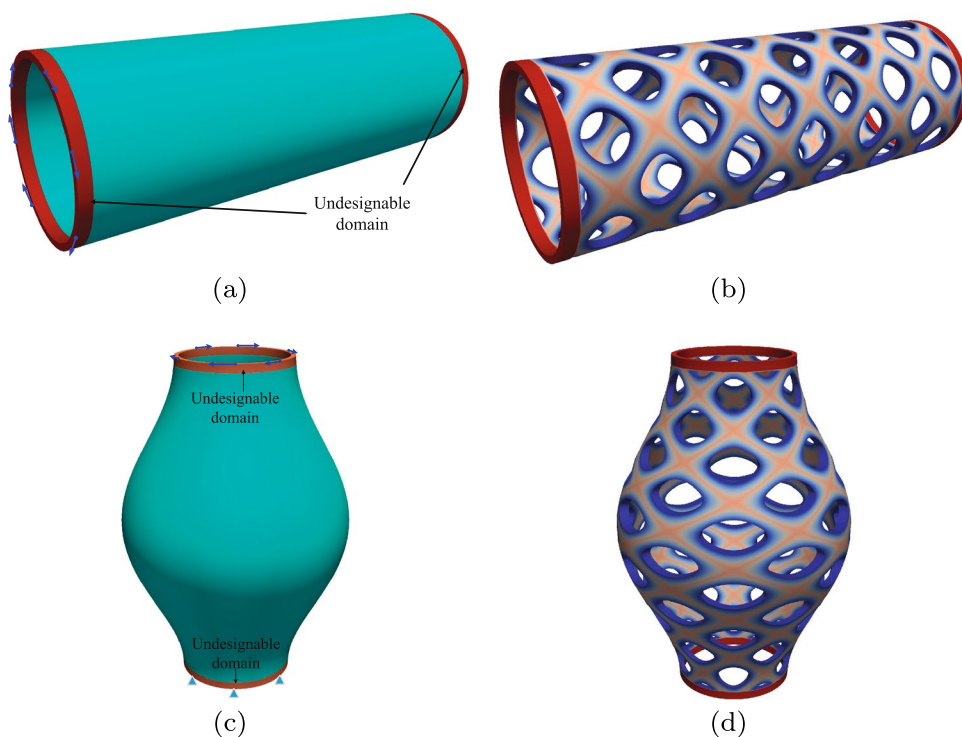
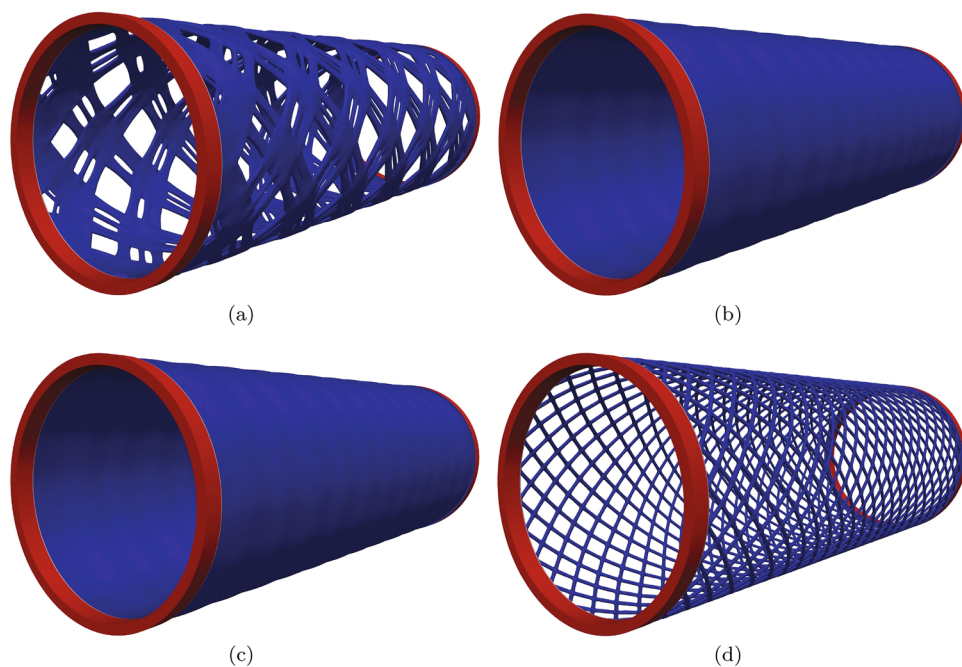


Fig. 16 Optimized structures with considering the repetition constraint: **a** number of repetition patterns along the circumferential direction $N_{patterns} = 6$; **b** $N_{patterns} = 12$; **c** $N_{patterns} = 24$; **d** $N_{patterns} = 24$ for a lower volume fraction upper limit $v_f = 0.15$



5 Conclusion

The level set method has been more and more widely used in the field of structural topology optimization since 2003, because of its obvious advantages, especially in describing complex geometric configurations. To overcome

some shortcomings of the classic level set method, the traditional parameterized level set method (PLSM) has been proposed since 2006 by using the radial basis functions (RBFs) to parameterize the level set function. However, an additional linear system needs to be solved during the parameterization process within each optimization iteration. The number of non-zero elements of the

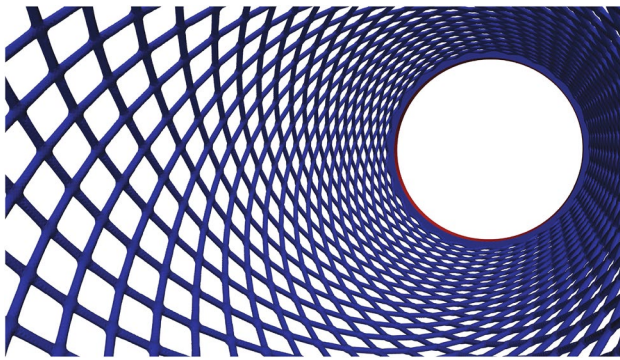


Fig. 17 Internal view of the optimized structure shown in Fig. 16d

parameterized matrix \mathbf{H} is closely related to the size of the support region of the GSRBFs or the CSRBFs. The parameterized matrix is full when using the GSRBFs to parameterize the level set function and it will become sparse when the CSRBFs are employed for the parameterization. No matter which kind of the RBFs is used for the parameterization, the additional linear system must be solved, which will consume a lot of computer memory and calculation time, especially for 3D large-scale/high-resolution structural topology optimization problems.

To further improve the calculation efficiency based on the traditional PLSM, the shape functions adopted in the FEM are employed herein to parameterize the level set function. After using the shape functions, the parameterization matrix \mathbf{H} will become an identity matrix, which completely avoids the solving of the above-mentioned additional linear system of the parameterization process. In this way, lots of computer memory and computing time will be saved when using the shape functions for parameterization. In addition, the shape functions are adaptive for any structured mesh or unstructured mesh, which keeps the parameterization

matrix \mathbf{H} always an identity matrix for the arbitrary shape of the design domain. Because of this, we call this proposed method an adaptive parameterized level set method. Furthermore, to verify the effectiveness of the proposed method in large-scale structural topology optimization problems, the calculation program is processed in parallel based on the PETSc, an open-source scientific computation platform.

Several numerical examples have been carried out for verifying the correctness and effectiveness of the proposed APLSM. By comparison with the traditional GSRBFs- or CSRBFs-based PLSM, we can see that the optimized configurations obtained by both the PLSM and APLSM are almost the same for the 2D and 3D problems. Based on the fully parallel computation technique, the calculation scale can theoretically be infinitely expanded as long as there are enough computer resources. In this paper, more than 13 million hexahedral elements are used for the optimization of the plate model. By analyzing the computing time, one can see that the efficiency of the proposed APLSM is very high. In the optimization problem of the plate model, except for the time cost in solving the linear system of structural analysis, only less than 2 s are consumed during the processes in each iteration including the mesh generation, the assembly of each element stiffness matrix, the calculation of the strain energy, the evolution of the level

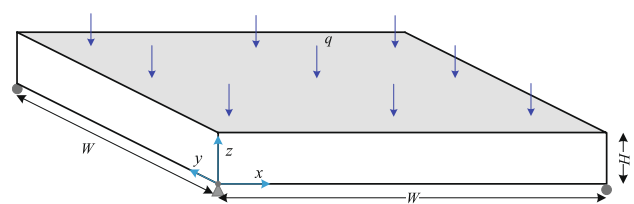
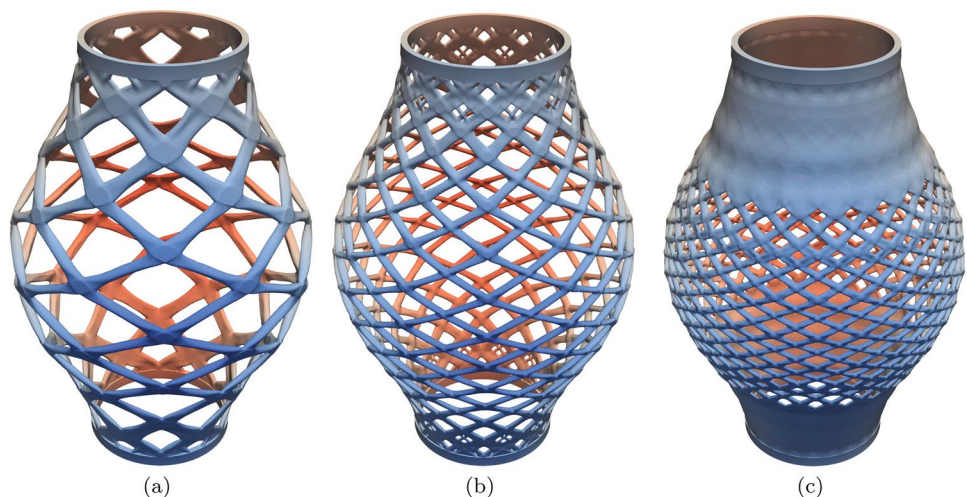


Fig. 19 Design domain and boundary conditions of the plate model with considering the repeat pattern constrains

Fig. 18 Comparison of the optimized vase-like structures: **a** number of repetition patterns is set as $N_{patterns} = 6$; **b** $N_{patterns} = 12$; **c** $N_{patterns} = 24$



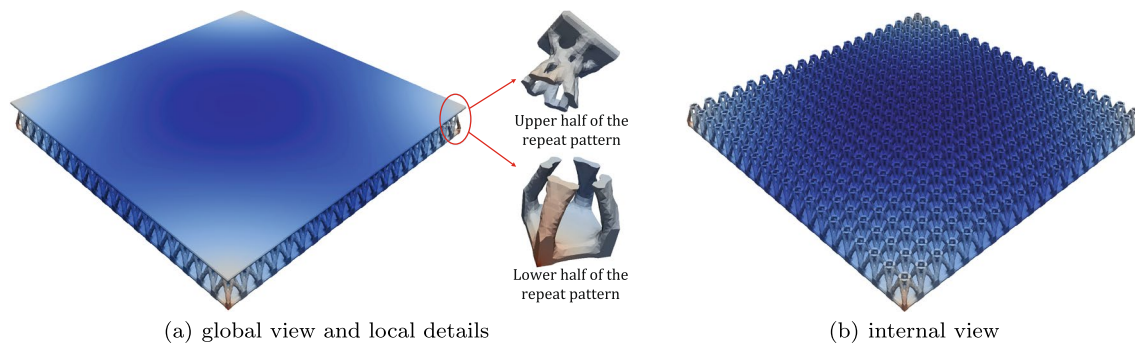


Fig. 20 Optimized plate considering the repeat pattern constraints

set function, etc. From the optimized structures, we can find that lots of very small structures, such as truss-like and thin shell components, will appear in the final designs. Besides, a repetition pattern constraint in this paper is successfully applied for optimizing the hierarchical and periodic cellular structures by using the proposed method and the parallel computing technique.

Acknowledgements This research work is supported by the National Natural Science Foundation of China (Grant Nos. 12072242, 12072114), the Natural Science Foundation of Hubei Province (Grant No. 2020CFB816), and the Opening Project of Guangdong Provincial Key Laboratory of Technique and Equipment for Macromolecular Advanced Manufacturing in South China University of Technology (Grant No. 2020kfk03).

Declarations

Conflict of interest The authors declare that they have no conflict of interest.

Replication of results The program code of the 2D optimization problem in this paper is written in matlab language. The code for the 3D problem is based on the PETSc open-source computing platform. All data in this article can be obtained under reasonable request.

References

- Allaire G, Jouve F, Toader AM (2004) Structural optimization using sensitivity analysis and a level-set method. *J Comput Phys* 194:363–393
- Bendsøe MP, Kikuchi N (1988) Generating optimal topologies in structural design using a homogenization method. *Comput Methods Appl Mech Eng* 71:197–224
- Burger M, Osher SJ (2005) A survey on level set methods for inverse problems and optimal design. *Eur J Appl Math* 16:263–301
- Chen L, Liu H, Chu X, Wang J (2021) Functionally graded cellular structure design using the subdomain level set method with local volume constraints. *Comput Model Eng Sci* 128(3):1197–1218
- Deaton JD, Grandhi RV (2014) A survey of structural and multidisciplinary continuum topology optimization: post 2000. *Struct Multidiscip Optim* 49:1–38
- Gain AL, Paulino GH (2013) A critical comparative assessment of differential equation-driven methods for structural topology optimization. *Struct Multidiscip Optim* 48:685–710
- Guo X, Zhang W, Zhong W (2014) Explicit feature control in structural topology optimization via level set method. *Comput Methods Appl Mech Eng* 272:354–378
- Ho HS, Wang MY, Zhou M (2007) Parametric structural optimization with dynamic knot RBFs and partition of unity method. *Struct Multidiscip Optim* 47:353–365
- Ho HS, Lui BFY, Wang MY (2011) Parametric structural optimization with radial basis functions and partition of unity method. *Optim Methods Softw* 26:533–553
- Jahangiry HA, Tavakkoli SM (2017) An isogeometrical approach to structural level set topology optimization. *Comput Methods Appl Mech Eng* 319:240–257
- Jiang L, Chen S, Jiao X (2018) Parametric shape and topology optimization: a new level set approach based on cardinal basis functions. *Int J Numer Methods Eng* 144:66–87
- Li H, Li P, Gao L, Zhang L, Wu T (2015) A level set method for topological shape optimization of 3D structures with extrusion constraints. *Comput Methods Appl Mech Eng* 283:615–635
- Liu Y, Li Z, Wei P, Wang W (2018) Parameterized level-set based topology optimization method considering symmetry and pattern repetition constraints. *Comput Methods Appl Mech Eng* 340:1079–1101
- Liu H, Zong H, Tian Y, Ma Q, Wang MY (2019) A novel subdomain level set method for structural topology optimization and its application in graded cellular structure design. *Struct Multidiscip Optim* 60:2221–2247
- Liu H, Tian Y, Zong H, Ma Q, Wang MY, Zhang L (2019) Fully parallel level set method for large-scale structural topology optimization. *Comput Struct* 221:13–27
- Liu H, Zong H, Shi T, Xia Q (2020) M-VCUT level set method for optimizing cellular structures. *Comput Methods Appl Mech Eng* 367:113154
- Luo Z, Tong L, Wang MY, Wang S (2007) Shape and topology optimization of compliant mechanisms using a parameterization level set method. *J Comput Phys* 227:680–705
- Luo Z, Wang MY, Wang S, Wei P (2008) A level set-based parameterization method for structural shape and topology optimization. *Int J Numer Methods Eng* 76:1–26
- Saad Y (1993) A flexible inner-outer preconditioned GMRES algorithm. *SIAM J Sci Comput* 14:461–469
- Sigmund O, Maute K (2013) Topology optimization approaches. *Struct Multidiscip Optim* 48:1031–1055
- Sigmund O, Aage N, Andreassen E (2016) On the (non-)optimality of Michell structures. *Struct Multidiscip Optim* 54:361–373

- van Dijk NP, Maute K, Langelaar M, van Keulen F (2013) Level-set methods for structural topology optimization: a review. *Struct Multidiscip Optim* 48:437–472
- Wang Y, Benson DJ (2016) Isogeometric analysis for parameterized LSM-based structural topology optimization. *Comput Mech* 57:19–35
- Wang S, Wang MY (2006) Radial basis functions and level set method for structural topology optimization. *Int J Numer Methods Eng* 65:2060–2090
- Wang MY, Wang X, Guo D (2003) A level set method for structural topology optimization. *Comput Methods Appl Mech Eng* 192:227–246
- Wang S, Lim KM, Khoo BC, Wang MY (2007) An extended level set method for shape and topology optimization. *J Comput Phys* 221:395–421
- Wang MY, Zong H, Ma Q, Tian Y, Zhou M (2019) Cellular level set in B-splines (CLIBS): a method for modeling and topology optimization of cellular structures. *Comput Methods Appl Mech Eng* 349:378–404
- Wei, P, Wang, MY (2006) Parametric structural shape and topology optimization method with radial basis functions and level-set method. In: *Proceedings of the ASME 2006 international design engineering technical conferences and computers and information in engineering conference*, pp. 10–13, Philadelphia, USA, September 2006
- Wei P, Li Z, Li X, Wang MY (2018) An 88-line MATLAB code for the parameterized level set method based topology optimization using radial basis functions. *Struct Multidiscip Optim* 58:831–849
- Wei P, Yang Y, Chen S, Wang MY (2020) A study on basis functions of the parameterized level set method for topology optimization of continuums. *J Mech Des* 143(4):041701
- Wendland H (1995) Piecewise polynomial, positive definite and compactly supported radial functions of minimal degree. *Adv Comput Math* 4:389–396
- Xia Q, Shi T (2015) Constraints of distance from boundary to skeleton: for the control of length scale in level set based structural topology optimization. *Comput Methods Appl Mech Eng* 295:525–542
- Xia Q, Shi T, Xia L (2019) Stable hole nucleation in level set based topology optimization by using the material removal scheme of BESO. *Comput Methods Appl Mech Eng* 343:438–452
- Yaghmaei M, Ghoddosian A, Khatibi MM (2020) A filter-based level set topology optimization method using a 62-line matlab code. *Struct Multidiscip Optim* 62:1001–1018

Publisher's Note Springer Nature remains neutral with regard to jurisdictional claims in published maps and institutional affiliations.